Identification of sulphur dioxide sources using in-situ measurements at a sub-urban site in the North-West Indo-Gangetic Plain

Nimya. S.S

MS 12067

A dissertation submitted for the partial fulfilment of

BS-MS dual degree in Science

Indian Institute of Science Education and Research Mohali

April 2017

Certificate of Examination

This is to certify that the dissertation titled **"Identification of sulphur dioxide sources using in-situ measurements at a sub-urban site in the North-West Indo-Gangetic plain"** submitted by Ms. Nimya. S.S (Reg. No. MS12067) for the partial fulfilment of BS-MS dual degree programme of the Institute, has been examined by the thesis committee duly appointed by the Institute. The committee finds the work done by the candidate satisfactory and recommends that the report be accepted.

Dr.Baerbel Sinha (Supervisor) Dr.Vinayak Sinha Dr.Sugumar Venkataramani

Dated: April 21, 2017

Declaration

The work presented in this dissertation has been carried out by me under the guidance of Dr. Bärbel Sinha at the Indian Institute of Science Education and Research Mohali.
This work has not been submitted in part or in full for a degree, a diploma, or a fellowship to any other university or institute. Whenever contributions of others are involved, every effort is made to indicate this clearly, with due acknowledgement of collaborative research and discussions. This thesis is a bonafide record of original work done by me and all sources listed within have been detailed in the bibliography.

Nimya. S.S

(Candidate)

Dated: April 21, 2017

In my capacity as the supervisor of the candidate's project work, I certify that the above statements by the candidate are true to the best of my knowledge.

Dr. Bärbel Sinha

(Supervisor)

Acknowledgement

Above all, my heart shall be raised in gratitude to the Almighty for his universal grace towards me. It is my pleasure to extend my deep sense of gratitude and indebtedness to my guide, Dr. Bärbel Sinha for her guidance and support. I owe my most sincere thanks to the Director, Prof.N. Sathyamurthy, IISER Mohali for providing the facility to carry out my thesis. I am thankful to Dr. Vinayak Sinha and Dr. Sugumar Venkataramani for providing their valuable inputs.

I thank the Department of Science and Technology for providing the INSPIRE fellowship.

I thank the IISER Mohali informatics centre for providing all the facilities.

I also acknowledge all my lab mates especially Saryu Garg, Harshita Pawar, B.Praphulla Chandra and Gaurav Sharma for their help and support at all times. I would also like to thank my friends T.H Anishya and Haritha. R, Ebin, Shabin and Bharti for providing me with continuous support and encouragement.

List of Figures

List of Tables

List of Abbreviations

CPCB ..... Central Pollution Control Board

EPA ..... Environment Protection Agency

NAAQS ..... National Ambient Air Quality Standard

IPCC ..... Intergovernmental Panel on Climate Change

ppbv ..... parts per billion volume

pptv ..... parts per trillion volume

DMS ..... Dimethyl Sulphide

CI ..... Criegee intermediate

sCI ..... Stabilized Criegee intermediate

REAS ..... Regional Emission Inventory in Asia

CRDS ..... Cavity Ring Down Spectroscopy

MAD ..... Median Absolute Deviation

NW-IGP ..... North-West Indo-Gangetic Plain

Contents

Abstract

Sulphur dioxide is an air pollutant that is emitted into atmosphere from both natural and anthropogenic sources. It is important to study and identify the sources of SO_2 since it has a huge impact on our climate. The sulphate aerosol which is formed by the oxidation of SO_2 has a radiative forcing of -0.4 Wm^{-2} and it results in a decrease in Earth's energy budget and thus brings a cooling effect.

Lu et al., casts doubt on the surface measurements of SO_2 in India because SO_2 levels have been reported to decrease at most Central Pollution Control Board (CPCB) monitoring sites after the introduction of sulphur free fuels while satellite observations provided evidence for an increasing SO_2 column over many regions.

Here we address the aforementioned discrepancy in the SO_2 emission trend using in-situ SO_2 and meteorological dataset measured at a sub-urban site in the North-West Indo-Gangetic Plain during 2015. We also seek to identify the major sources of SO_2 over this region.

The strongest sources of SO_2 measured at our site were found to be the three coal fired power plants located in the North-West, South-East and South-West directions and there was a minor contribution from traffic as well.

Chapter 1

INTRODUCTION

Sulphur dioxide is a pollutant that is emitted into the atmosphere from natural and anthropogenic sources. It is mainly emitted from fossil fuel combustion and other industrial facilities.[1] It is one of the six criteria air pollutants identified by the Environment Protection Agency (EPA) which are known to be harmful to public health and environment. The National Ambient Air Quality Standard (NAAQS) for SO_2 mixing ratio in India is 30 ppbv for 24 hour average and 19 ppbv for annual average. At our site, it has never exceeded the NAAQS limits.

As a result of the chemical reaction of sulphur oxides with water (in water droplets or in gas phase), acid rain occurs.[2] The acid deposition includes acidity caused by wet and dry deposition of SO_2 gas in the forest environment. The dry deposition of SO_2 contributes to acid rain because SO_2 which was dry deposited to the leaf surface gets oxidised to acid after entering the stomata or on the leaf surface during rain episodes. Acid rain is not a serious problem in India as the acidity is buffered by soil calcium and the biomass burning potassium and ammonia emission. The anthropogenic emissions of SO_2 occurs during the combustion of coal for energy production in the power, industrial, transport and residential sectors.

1.1 Climatic impact of SO_2

The balance between the incoming solar radiation and the outgoing infra-red radiation determines the surface temperature of Earth. The radiative forcing of a gas is defined as the flux imbalance caused by the increase in concentration of that gas. Positive radiative forc-

ing increases the Earth's energy budget and leads to warming whereas negative radiative forcing results in a decrease in Earth's energy budget and leads to cooling.[3]

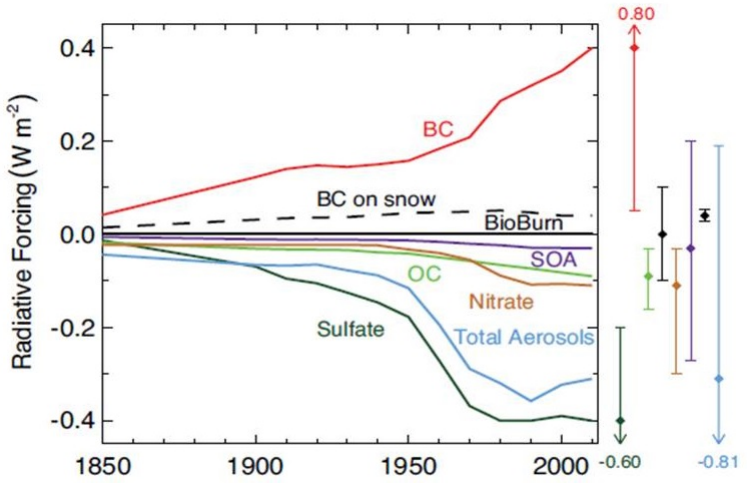

Figure 1.1: Time evolution of radiative forcing due to aerosol radiation interaction (Reproduced with permission from Intergovernmental Panel on Climate Change Assessment Report 5, Chapter 8, Page No:683[4])

Sulphate aerosol is effective in the scattering of short wave radiation and results in cooling of the lower troposphere.[5] According to the IPCC (Intergovernmental Panel on Climate Change) Assessment Report 5, the global mean radiative forcing of sulphate aerosol from 1750 to 2011 is -0.4 Wm^{-2}.[4] Volcanic eruptions are the dominant natural reason for the forced climate change because of the injection of large amounts of SO_2 gas. In 1991, the volcano Mount Pinatubo in Philippines erupted and injected 15 to 30 MT of SO_2 into the stratosphere. SO_2 was converted into sulphuric acid, which condensed into sulphate aerosol in a month.[6] In 1815, the volcano Tambora in Indonesia erupted and released 53 to 58 Tg of SO_2. This got converted to around 93 Tg of sulphate aerosol which resulted in a radiative cooling of 6 $Wm^{-}2$ and a global cooling of 1 to 1.5 °C.[7]

1.2 Sources and Sinks of SO_2

1.2.1 Sources

Sulphur dioxide has both natural and anthropogenic sources. Natural sources include volcanic eruptions, DMS (dimethyl sulfide) emitted by marine phytoplanktons, wildfires etc. and anthropogenic sources include combustion of sulphur containing fossil fuels, industries

such as brick kilns, steel industry etc.[8] Total global distribution of SO_2 is 206 Tg per year. Oxidation of DMS accounts for about 19.4% of total SO_2 emissions. 72.8% is fossil fuel derived and 7.7% comes from the volcanoes.[9] DMS is an important source of SO_2 in the

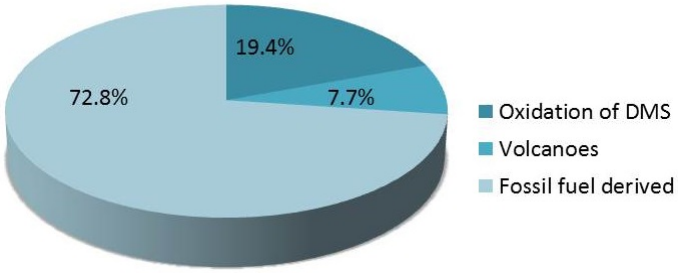

Figure 1.2: Sources of SO_2.[9]

marine atmosphere. It is produced by macro and micro-algae. Dimethylsulphoniopropionate (DMSP) is the precursor of DMS.[10] This molecule contains a 1:1 ratio of DMS and acrylic acid. In the atmosphere the attack of DMS by OH and NO_3 radicals yields SO_2.
The rapid economic growth in the Asian countries have experienced a growth in energy consumption. More than 80% of all energy is derived from fossil fuels. The dominant energy source is coal and is expanding at a rate of 6.5% per year.[2] As a consequence SO_2 emissions over India have increased.

1.2.2 Sinks

SO_2 is removed form the atmosphere mainly by dry deposition, wet deposition, gas phase oxidation and aqueous phase oxidation.[9] It is estimated that 37% of SO_2 is removed by dry deposition, 33% by aqueous phase oxidation, 17% by wet deposition and 13% by gas phase oxidation.[11] In the gas phase, SO_2 is oxidised by OH radicals and Criegee intermediates and in the aqueous phase by hydrogen peroxide (H_2O_2) and ozone (O_3).

1.3 Gas phase oxidation of SO_2

SO_2 gets oxidised in the gas phase mainly by hydroxyl radicals (OH) and stabilized Criegee intermediates (sCI).

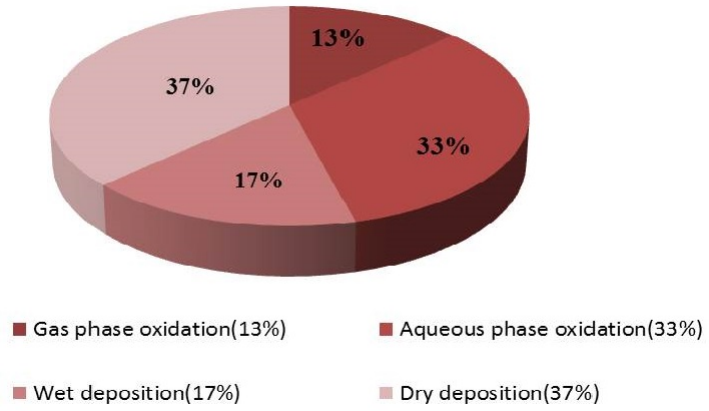

Figure 1.3: SO_2 sink budget.[11]

1.3.1 Hydroxyl radical

The predominant mechanism for the conversion of SO_2 to H_2SO_4 is a homogenous gas phase oxidation of SO_2. The reaction is considered to proceed via the following scheme:

$$SO_2 + OH + M \longrightarrow HSO_3 + M \qquad \dashrightarrow (1)$$

The OH will add to the molecule at the sulphur atom. This is a termolecular reaction and at 1 atm this is in the fall off region between second and third order. The high pressure limiting rate constant for reaction (1) at room temperature is $k_\infty = 2\times10^{-12}$ cm ^{3} molecule^{-1} s^{-1} and the low pressure rate constant is $k_o = 4\times10^{-31}[N_2]$cm^6 molecule^{-2} s^{-1}.[12]
The effective bimolecular rate constant is $k_4^{bi} = 9.7\times10^{-13}$ cm ^{3} molecule^{-1}s^{-1}.

$$HSO_3 + O_2 \rightarrow SO_3 + HO_2 \qquad \dashrightarrow (2)(\text{fast})$$

This is a fast reaction and the rate constant is $k = 4.3\times10^{-13}$ cm^3 molecule^{-1} s^{-1} at room temperature.The lifetime of $HOSO_2$ adduct is thus 0.5 μs at 1 atm in the air.[12]

$$SO_3 + H_2O + M \longrightarrow H_2SO_4 + M \qquad \dashrightarrow (3)$$

The stable sulphur trioxide molecule rapidly combines with a gaseous water molecule to form sulphuric acid. Finally, the H_2SO_4 reacts with water, whether in the form of water vapour or as a mist, to form an aerosol.
The most important source of OH radicals are the photolysis of O_3 in the presence of water

vapour as depicted in the reactions below:

$$O_3 + hv \rightarrow O^* + O_2 \dashrightarrow (4)$$
$$O^* + H_2O \rightarrow OH + OH \dashrightarrow (5)$$

where hv represents a radiation photon. Another source of OH radicals is through the photolysis of formaldehyde (HCHO), which produces hydroperoxy radicals HO_2. Through reactions with NO and O_3, HO_2 radicals are rapidly recycled to OH radicals[13] (equations 9,10).

$$HCHO + hv \rightarrow H + HCHO \qquad \dashrightarrow (6)$$
$$H + O_2 + M \rightarrow HO_2 + M \qquad \dashrightarrow (7)$$
$$HCO + O_2 \rightarrow HO_2 + CO \qquad \dashrightarrow (8)$$
$$HO_2 + NO \rightarrow OH + NO_2 \qquad \dashrightarrow (9)$$
$$HO_2 + O_3 \rightarrow OH + O_2 + O_2{}^{13} \qquad \dashrightarrow (10)$$

1.3.2 Criegee's Intermediate

Criegee intermediates are intermediate species formed in the reactions of unsaturated hydrocarbons with ozone.[14] It can play an important role in tropospheric oxidation. Ozonolysis of alkenes is the first step in the formation of Criegee intermediate radicals. The reaction forms a primary ozonide with high excess energy. Due to the excess energy, primary ozonide decompose instantaneously to the Criegee intermediate, which still possess excess energy. The Criegee intermediate either decompose into different products or collisionally stabilize (latter is referred as a stabilized Criegee intermediate, sCI) to liberate it's excess energy. The sCI can then react with H_2O, NOx, SO_2, CO and many others[15]

The rate constant for the reaction of sCI with SO_2 is 3.9×10^{-11} cm ^{3} molecule^{-1} s^{-1} which is faster than previously reported rates.[16]

Based on a model study by M.Boy et al, the contribution from sCI to the production of sulphuric acid is most important in the canopy, where the concentrations of organic compounds are the highest. But their overall result shows that upto 100 m, the effect of sCI is very important.

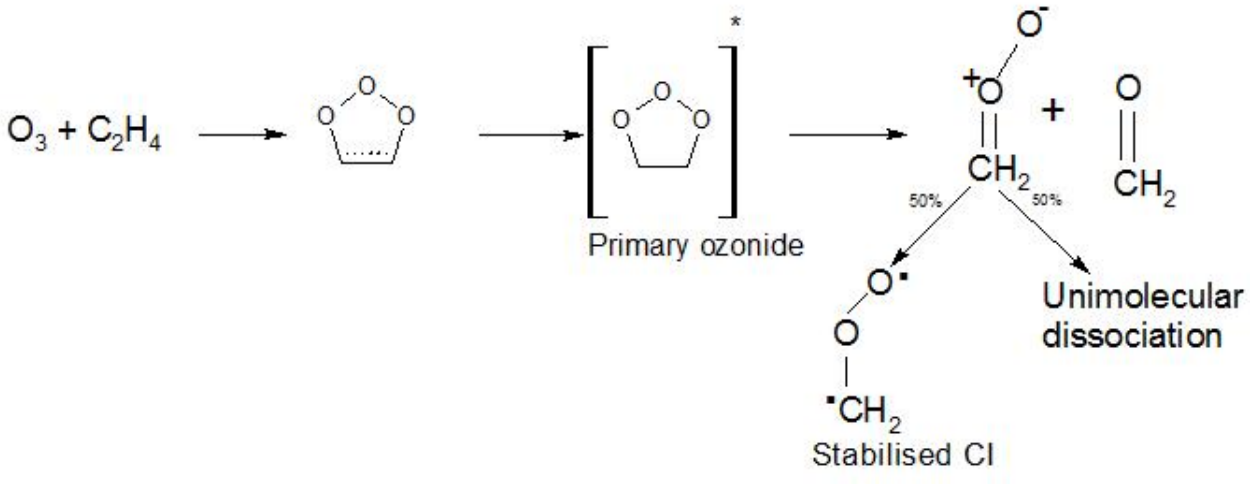

Figure 1.4: Reaction mechanism of ozonolysis of ethylene[15]

The ozonolysis of isoprene contributes around 62% for the production of criegee intermediates, the ozonolysis of monoterpenes is responsible for about 23% of the criegee intermediates, and the rest (13%) is from the ozonolysis of propene.[16]

1.4 Aqueous phase oxidation of SO_2

1.4.1 S(IV) aqueous equilibria

Sulphur dioxide gas dissolves in water to set up the following equilibria:

$$\mathrm{SO_2(g) + H_2O \leftrightharpoons SO_2.H_2O} \qquad \mathrm{H_1 = 1.242 Matm^{-1}}$$
$$\mathrm{SO_2.H_2O \leftrightharpoons HSO_3^- + H^+} \qquad \mathrm{K_2 = 1.32 \times 10^{-2} M}$$
$$\mathrm{HSO_3^- \leftrightharpoons SO_3^2 - + H^+} \qquad \mathrm{K_3 = 6.42 \times 10^{-8} M}$$

The dissolved SO_2 includes three chemical species: hydrated SO_2, the bisulfite ion (HSO_3^-), and the sulfite ion (SO_3^{2-}). The acidity of the solution in which SO_2 dissolves determines the predominant species dissolved. S(IV) is mainly in the form of $SO_2.H_2O$ at pH values lower than 2. At higher pH values, the HSO_3^- fraction increases, and in the pH range from 3 to 6 practically all S(IV) occurs as HSO_3^-. At pH values higher than 7, SO_3^{2-} dominates. If a chemical reaction occurs in solution involving either, the rate of reaction will depend on pH since the concentration of these species depends on pH.[12]

1.4.2 Oxidation of S(IV) by dissolved ozone

In contrast to the gas phase reaction, the aqueous phase reaction of ozone with SO_2 is rapid.

$$O_3 + S(IV) \rightarrow S(IV) + O_2$$

The rate of the reaction of S(IV) with dissolved ozone for a dilute solution is:

$R_0 = (k_0[SO_2.H_2O] + k_1[HSO_3^-] + K_2[SO_3^{2-}])[O_3]$

with $K_0 = 2.4 \pm 1.1 \times 10^4\ M^{-1}\ s^{-1}$

$k_1 = 3.7 \pm 0.7 \times 10^5\ M^{-1}\ s^{-1}$

$k_2 = 1.5 \pm 0.6 \times 10^9\ M^{-1}\ s^{-1}$

1.5 Emission scenario in India

REAS 2.1 emission inventory estimates a total emission of 56.9 Tg of SO_2 in 2008 from Asia. The majority of Asian SO_2 emissions during the period 2000–2008 come from China, followed by India. Around 40% of the global anthropogenic SO_2 emissions are from Asia.[17] The Asian SO_2 emissions increased from 2000- 2006 and then began to decrease because of the installation of flue gas desulfurisation techniques in the coal fired power plants in China. The second largest contributor to Asian emissions is India because of the rapid increase in the consumption of fossil fuels, industrial production and the increase in the number of vehicles.[18]

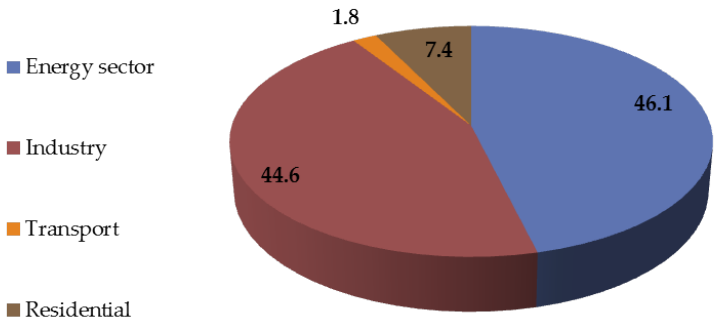

Figure 1.5: Sector wise emissions of SO_2 in India in 2011.[19] Numbers represents the percentage contributions of each sector.

Figure1.5 shows the sector wise emissions of SO_2 in Indian in 2011. The total emissions of SO_2 in 2011 was 10.1 Tg. Out of which around half of the emissions were from the energy sector. There was an increase of 53% in the growth rate between 2000 to 2008. The increase in growth rate was due to the increase in power plant emissions from 2000 to 2008.[18]

1.6 Definition of the problem

A recent study by Lu et al., reported a discrepancy in the measurements of SO_2 emissions over India. They compared the SO_2 emissions and the Ozone Monitoring Instrument (OMI) SO_2 observations over Indian coal-fired power plants. OMI observed a 63% increase in the total amount of SO_2 observed between 2005 to 2012 whereas the national mean of SO_2 reported by Central Pollution Control Board (CPCB) showed a decreasing trend. They conclude that *"Current government reports and statistics may give a misleading impression that the SO_2 situation is improving"*[8](Lu et al., page no:13998, line no:52) and subsequently recommend that *"The network of CPCB NAMP station needs to be optimized to reflect the true SO_2 situation across the country"*[8](Lu et al., page no: 13998, line no:56).
My thesis proposes to investigate this apparent discrepancy in the measurement of SO_2 emissions using in-situ data from a site surrounded by three power plants.

Chapter 2

Materials and Methods

2.1 Site description

I use 1 year data (from January 1 to December 31 2015) of SO_2, Carbon monoxide (CO) and Carbon dioxide (CO_2) measured at the Atmospheric Chemistry facility of IISER Mohali (30.667° N, 76.729° E; 310 m a.s.l.). Pulsed UV Fluorescence technique using a Thermo Fischer Scientific 43-i trace level analyzer at IISER Mohali-Ambient air quality station was used to carry out the measurement of SO_2 . Gas filter correlation (GFC) non-dispersive infrared (NDIR) technique using a Thermo Fischer Scientific 48-i trace-level enhanced analyzer was used for CO measurements. CO_2 measurements were carried out using Picarro G2508 Cavity Ring Down Spectrometer gas analyzer.

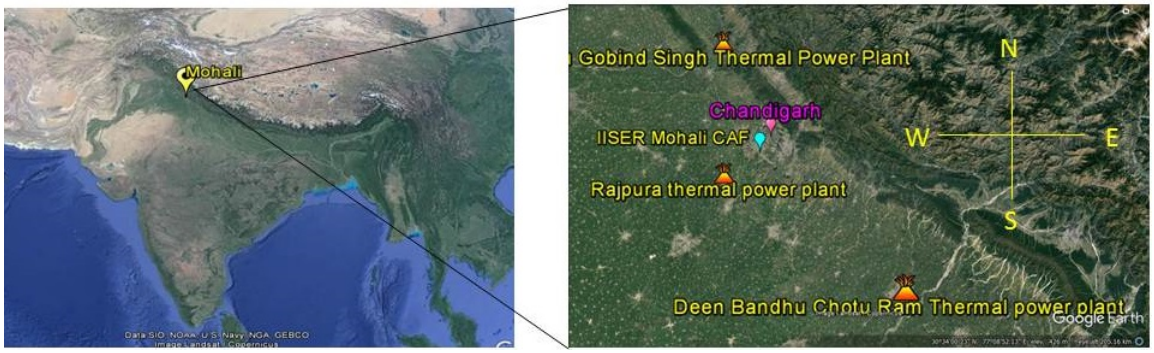

Figure 2.1: (Left) Location of Mohali (30.6670 N, 76.7290 E, 310 m.a.s.l.) in the NW-IGP. (Right) Exact location of the measurement facility and its spatial relationship with respect to the nearby cities and the mountain range.[Source- Google earth]

Figure 2.1 (left) shows the location of the city of Mohali in the north-western Indo-Gangetic Plain. The observations were carried out at the atmospheric chemistry facility

(CAF building) of IISER (a sub-urban site in the city Mohali). Figure 2.1 (right) shows the precise location of the measurement facility and its spatial relationship with respect to neighbouring cities.

The campus is situated several kilometres away from the nearest neighbour cities Mohali, Chandigarh and Panchkula. Chandigarh is the largest urban area near the site, which lies in the wind sector spanning from North to East (0 to 90°). The land use in the wind sector East to South (90 to 180°) of the site comprises of both agriculture and small industries (glass manufacturing, pharmaceuticals, solvent, etc.) in areas such as Zirakpur, Dera Bassi and Ambala. This wind sector includes Deenbandhu Chottu Ram thermal power station (110 km South East of the site), Mohali International Airport (8.5 km East of the site) and Bharat gas oil refinery (23 km South East of the site). The wind sector spanning from South to Northwest (180 to 270°)is mainly rural and agricultural land. This wind sector includes Rajpura village 1400 MW thermal power plant (first block commissioned in February 2014) 20 km South west (215°). From 270° to, 360° the land use is mainly rural and agricultural. This wind sector includes Guru Gobind Singh Thermal power plant (45 Km North-West of the site).[20]

2.2 General Meteorology

The meteorological parameters such as ambient temperature, relative humidity, wind speed, wind direction and solar radiation are measured at a meteorological station using meteorological sensors at a temporal resolution of 1 minute. All the instrument inlets and the meteorological sensors are co-located and placed at a measurement height of 20 m a.g.l. Figure 2.2 shows the wind rose plots of different seasons for the period of study: January 1 to December 31, 2015. Wind direction was mostly north to north-west ($270°C$-$360°C$ throughout the year except for monsoon period in which direction changes to south-east ($90°C$-$180°C$). Higher wind speeds (14 m/s) were observed during summer and monsoon period. Figure 2.3 shows the daily average of meteorological parameters such as the solar radiation, ambient temperature and relative humidity for the study period. The climate at this site is divided into four main seasons: Summer (March to June), Monsoon (July to mid-September), Post-monsoon (mid-September to November) and Winter (December to

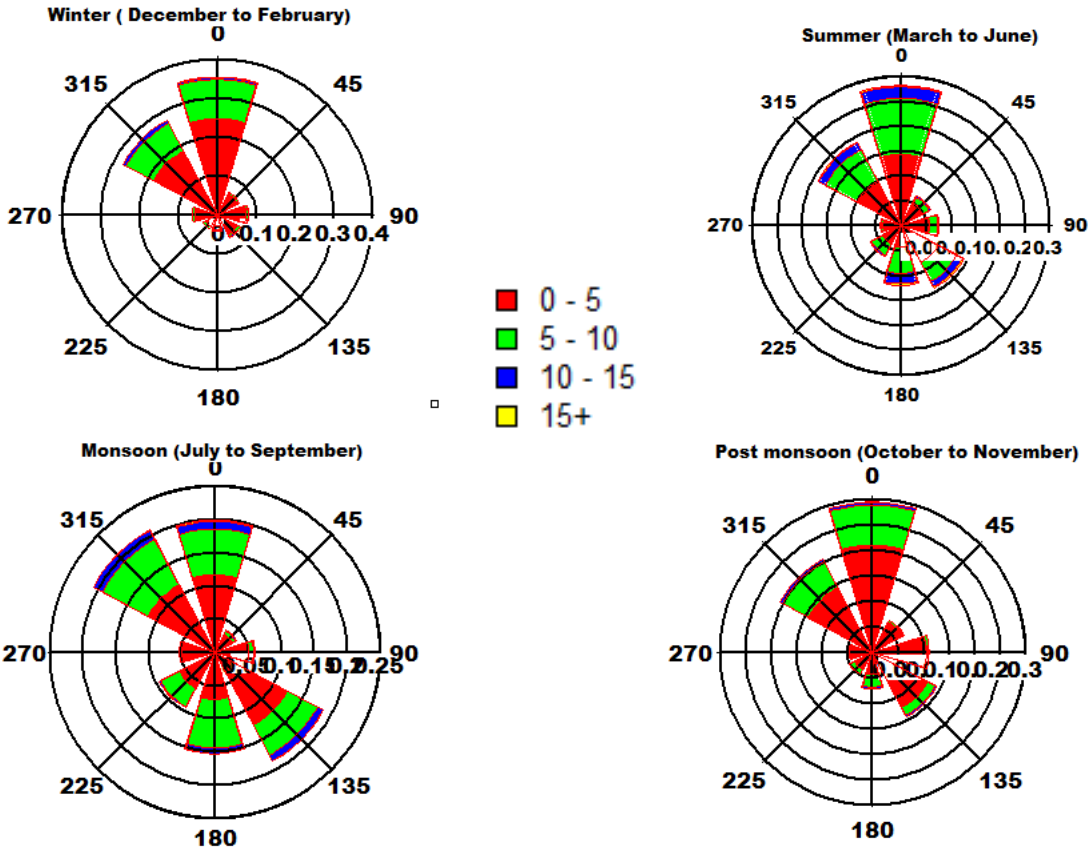

Figure 2.2: Wind rose plot for winter (December-February), Summer (March-June), Monsoon (July-September), Post-monsoon (October-November) seasons for the year 2015.

February) based on the variation in temperature, relative humidity, rainfall and solar radiation. The onset of winter time is defined to be when the daily temperature minima fell below $10°C$ and solar radiation maxima fell below 500 Wm^{-2}. Summer is characterised by high day time temperatures (>$40°C$), intense solar radiation and dry conditions (< 40% RH). Figure 2.4 shows the variability trend in SO_2 for the year 2015. Average values remain below 7 ppb in this region. Minimum values of SO_2 were observed during December and January as most of the SO_2 is oxidised in the fog which acts as an aqueous phase medium and maximum values were observed during summer and polluted post monsoon period due to dry conditions and thus the lack of aqueous phase sink of SO_2.

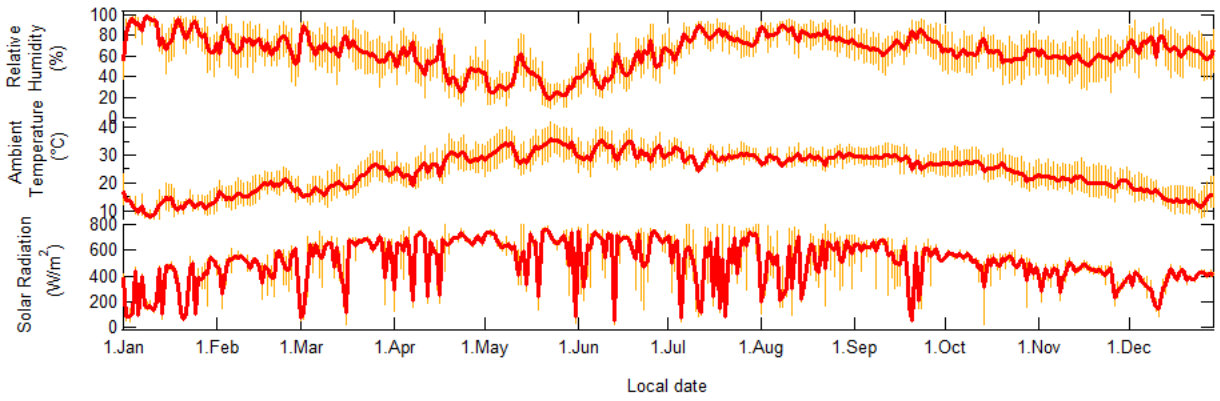

Figure 2.3: Daily average trend of Ambient Temperature ($°C$)(middle panel), Relative Humidity (%)(top panel) and peak daytime (12:00-14:00h) solar Radiation (Wm^{-2})(bottom panel). Vertical bars indicate variability as 10 and 90 percentiles and solid line represents daily average.

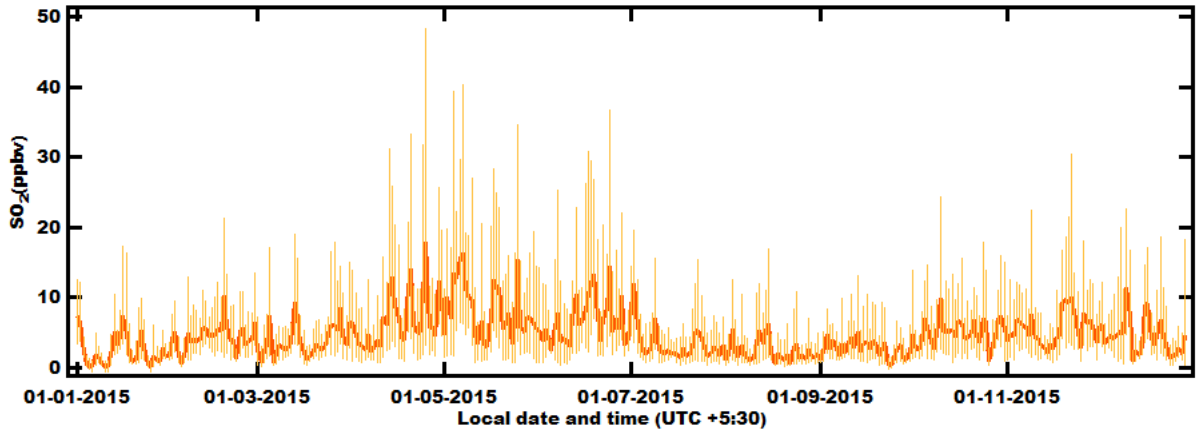

Figure 2.4: Variation in the SO_2 concentrations for the year 2015. Solid lines represents the daily average and the vertical bars indicate variability as 10 and 90 percentiles

2.3 Measurement of SO_2

The model 43i Thermo Fischer Scientific at Ambient Air Quality station IISER Mohali is used to determine the concentration of sulphur dioxide present in the ambient air which is generally present at ppbv levels over this region.

2.3.1 Principle of detection

The measurement of sulphur dioxide is based on fluorescence spectroscopy principles. The SO_2 molecules become excited at one wavelength when they are irradiated with UV radiation and then decay to a lower energy state emitting UV light at a different wavelength.[21]

$$SO_2 + hv_1 \rightarrow SO_2{}^* \rightarrow SO_2 + hv_2$$

Where, hv_1 = intensity of incident light

hv_2 = intensity of light during emission

SO_2 = SO_2 present in the ground state

SO_2 = SO_2 present in the excited state

By exciting SO_2 at 214 nm (absorption maxima) and measuring the intensity of fluorescence at 350 nm (emission maxima), SO_2 concentration can be measured. For the measurement of low concentration of SO_2, excitation by pulse UV light is more useful as compared to a continuous source.

2.3.2 Working Schematic

The sample is drawn inside the instrument via the bulkhead as shown in figure. There is a hydrocarbon kicker which permeates all the hydrocarbon molecules through the walls of tube so that only SO_2 molecules are allowed to enter inside. After that SO_2 molecules goes to Fluorescence chamber where pulsating UV radiation is coming from UV flash lamp (Zinc discharge lamp) and the condensing lens is used to focus the light. There is assembly of four mirrors and they reflect radiation of only that wavelength which can excite SO_2 molecules.

As the sample passes through this fluorescence chamber SO_2 molecules get excited. When SO_2 molecules relax to a lower energy state, they emit UV light having intensity proportional to concentration of SO_2. The band pass filter allows only the wavelength emitted by excited SO_2 molecules to reach the photo multiplier tube which detects the intensity of light at reflected wavelength. A reference detector monitors the emission from the Zinc lamp and is used to correct for fluctuations in lamp intensity. The detection limit is 1 ppb for 60 s average. The sample leaves the optical chamber and passes through flow sensor, capillary tube, hydrocarbon kicker and goes out through the exhaust bulk head.

2.3.3 General Interference problem

There are some species which can interfere with the ambient SO_2 measurement process.
1.Hydrocarbons : Cyclic hydrocarbons such as Naphthalene which are present at moderate

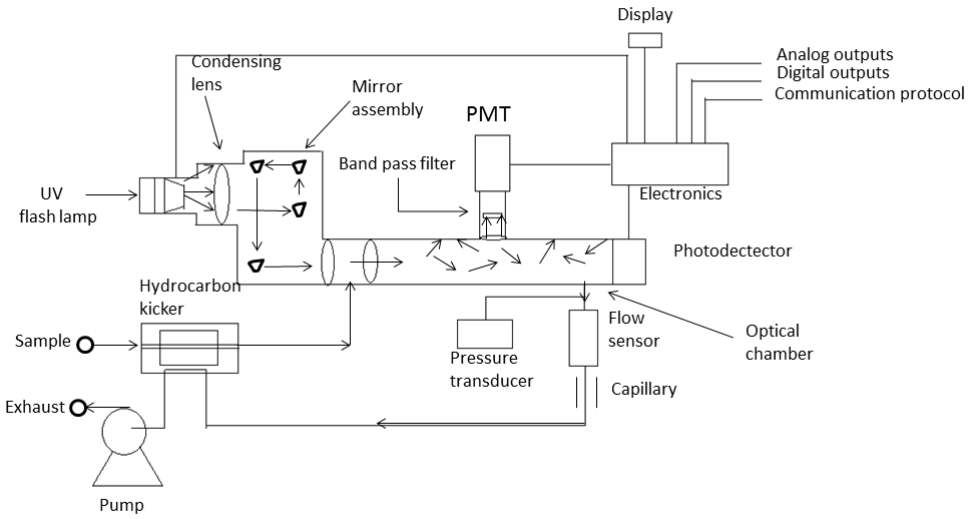

Figure 2.5: Schematic of model 43-i trace level SO_2 analyser.

to high concentrations in polluted areas shows strong fluorescence in the same spectral region as of SO_2. Thus it is important to remove these hydrocarbons and they can be removed by using hydrocarbon kicker.[22] Hydrocarbons diffuse through the wall of the membrane due to the differential partial pressure maintained by the sampling pump.

2.Water : As the hydrocarbon kicker removes only hydrocarbons, other molecules like water vapour and oxygen molecules can cause interference problem. Water vapour can be removed by using a dryer within the instrument or by careful selection of the incident radiation wavelength.

3.NO_x : Nitric oxides also show Fluorescence in the similar spectral range as that of SO_2. To avoid this problem band pass filters are used which allow only wavelengths emitted by excited SO_2 molecules to reach the PMT.

2.3.4 Data quality assurance

To ensure data quality, we do regular quality assurance measures. Zero air calibration is done once in a week, and a five-point span calibration is performed once in a month. Five point calibration in the dynamic range of 10-50 nmolmol^{-1} were performed using custom

Table 2.1: Zero drifts calibration done by me for SO_2 analyzer at AAQS, IISER Mohali

Sr.No.	Date	Time	Previous value	Zero drift	New value
1	17-08-2016	09:54-11:02	5.87	-0.60	5.27
2	26-08-2016	10:01-10:48	5.16	1.21	6.37
3	29-08-2016	16:24-17:44	6.57	-0.30	6.27
4	19-11-2016	15:50-16:40	6.38	0.03	6.41
5	03-12-2016	16:32-17:10	6.42	-0.32	6.10
6	01-03-2017	20:14-20:35	6.05	1.12	7.17
7	07-03-2017	19:27-19:50	7.18	-0.77	6.41
8	14-03-2017	15:28-16:37	6.45	-0.47	5.98
9	15-03-2017	15:16-15:44	4.97	0.19	5.15

Table 2.2: Span calibrations done by me for SO_2 analyzer at AAQS, IISER Mohali

Sr.No.	Date	Slope	Uncertainty in slope	Intercept	Uncertainty in intercept	R^2
1	26-08-2016	0.971	0.017	-2.614	0.553	0.997
2	19-11-2016	1.001	0.035	-11.395	1.06	0.998
3	14-03-2017	1.174	0.109	-4.788	3.41	0.974
4	07-04-2017	0.723	0.018	0.013	0.574	0.998

ordered standards. For calibration and zero drift characterization, a multi-gas calibrator and zero air generator equipped with a two stage scrubber (purafil and activated charcoal) and catalytic converter for generating ultra pure air were used. The drift is adjusted after getting a stable response for at least 10 minutes. All the zero drifts performed during the period Aug 2016- April 2017 has been shown in the table. The detection limit of the instrument was calculated as the 2 sigma error while passing zero air through the analyser. The systematic errors include 2% accuracy error inherent in the calibration gas standard, the 2σ instrumental precision error while measuring SO_2 at lowest calibration point and the flow uncertainty of 2% for each mass flow controllers used during the calibration. The total uncertainty was calculated using the root mean square propagation of individual uncertainties mentioned above and it comes out to be 5.77%.

The 2σ of measured values is defined as the detection limit of the instrument when zero air is passed through the analyser. For span calibration, five different known concentrations of

SO_2 are introduced through the analyser and the corresponding response is noted as shown in figure 2.6. 10, 20, 30, 40, and 50 ppb of SO_2 are introduced into the analyser, and a calibration curve is plotted as shown in figure. The slope of this curve is adjusted as the new coefficient in the analyser.

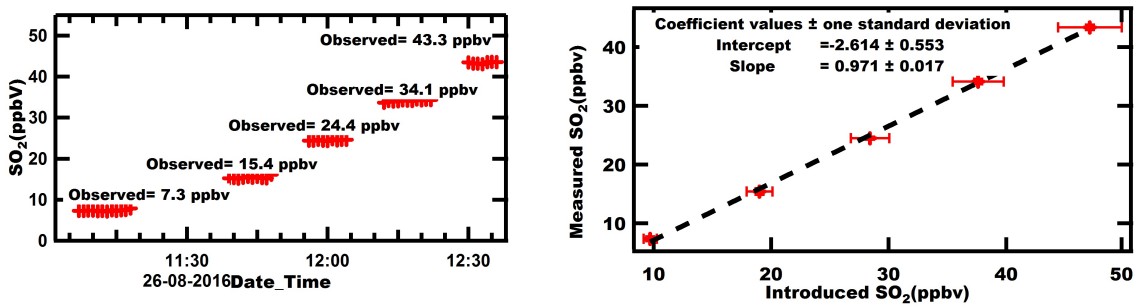

Figure 2.6: (Left) Plot of observed values of SO_2. (Right) Calibration curve showing linearity of SO_2. Vertical bars represent precision error and horizontal bar represents accuracy error.

2.4 Measurement of Carbon monoxide(CO)

The gas filter correlation (GFC) non-dispersive infra-red (NDIR) technique using a Thermo Fischer Scientific 48-i trace-level enhanced analyser was used for the measurement of carbon monoxide (CO).

2.4.1 Principle of operation

The model 48-i operates on the principle that carbon monoxide absorbs infra-red radiation at a wavelength of 4.6 microns.

2.4.2 Working Schematic

The sample which is drawn in through the sample bulk head reaches the optical bench. The radiation from an IR source is cut and then passed through a gas filter alternating between CO and N_2 by means of a rotating wheel. The radiation then passes through a narrow band pass interference filter and enters the optical bench where absorption by the sample gas occurs. The infra-red radiation then exits the optical bench and falls on an infra-red detector. The IR radiation passing through CO gas filter is used as a reference beam

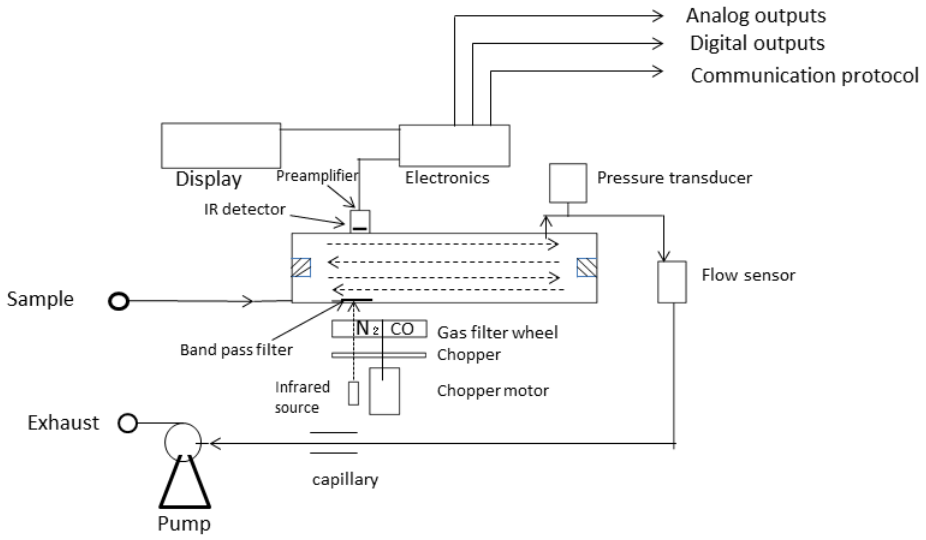

Figure 2.7: Flow schematic of model 48-i trace-level CO analyser.

whereas that passed through the N_2 side is used as a sample beam. The CO gas filter acts to produce a reference beam, which cannot be further attenuated by CO in the sample cell. The chopped detector signal is modulated by the alternation between the two gas filters with an amplitude related to the concentration of CO in the sample cell. Other gases absorb the reference and measure beams equally, they do not cause the modulation in detector signal. Thus, the GFC system responds specifically to CO.

2.5 Measurement of Carbon dioxide (CO_2)

CO_2 was measured by Picarro G2508 Cavity ring down spectrometer gas analyser. Cavity Ring Down Spectroscopy is a sensitive spectroscopic technique that makes use of an optical cavity to measure absorptions on the order of parts per million and beyond.

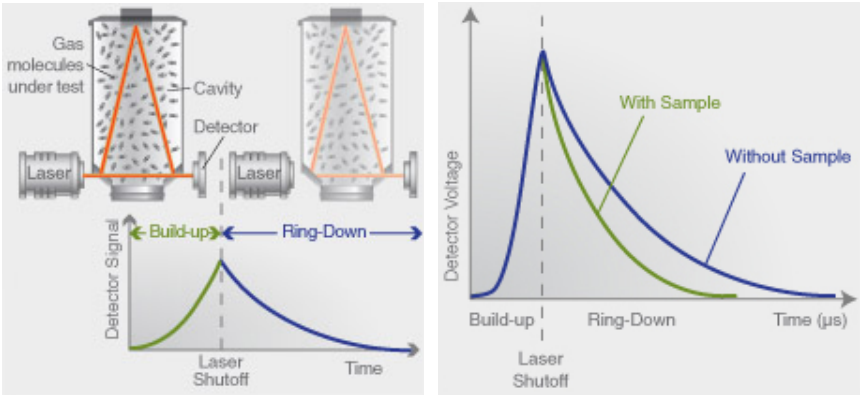

Figure 2.8: (Left)Schematic of Picarro CRDS analyser showing how a ring down measurement is carried out. (Right) Light intensity as a function of time with and without a sample having resonant absorbance.[23]

2.5.1 Working Principle

PICARRO CRDS consists of a laser beam emitting a single frequency beam and three mirrors called ring down mirrors. The beam from laser enters a small optical resonating cavity containing the analyte gas. When the build up is complete, the laser is shut off. The time taken for the light intensity to completely decay without the presence of any gas is called ring down time. When gas molecules are present, the decay will be faster according to Beer- Lambert's law (figure 2.8). Light circulates in the cavity many times, travelling 20 km or more. The high precision (parts-per-trillion detection levels) of CRDS comes from this long path length. A photo detector placed behind this mirror, senses the small amount of light leaking through the mirror to produce a signal that is proportional to the intensity in the cavity. In an empty cavity the only loss mechanisms are the mirrors. When the gas is present, the rotational vibrational modes provide additional loss mechanisms and the ring down time gets shorter proportional to the gas concentration. This difference in ring down time with the presence and absence of gas molecules is used to calculate back the concentration of species.

Chapter 3

Results and Discussions

3.1 Data processing and identification of SO_2 plumes

I use one year data (from January 1 to December 31, 2015) of SO_2 to carry out my work. To separate the SO_2 plumes from the baseline, I used robust statistics. Table 3.1 shows the robust statistical parameters such as the median and median absolute deviation (MAD). A 3σ outlier limit was applied, and we got SO_2 plumes as those having SO_2 concentrations greater than 7 ppbv. Data analysis were carried out using these filtered plumes. Figure 3.1 shows the time series of SO_2 before and after the separation of plumes for the month April.

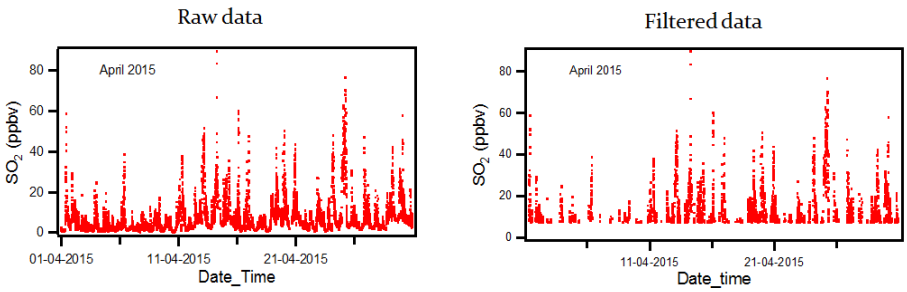

Figure 3.1: (Left) shows the time series of unprocessed SO_2 and (Right) shows the plume events for the month April 2015.

Table 3.1: Robust statistical analysis of data

Median	2.55
MAD	1.49
3σ outlier limit	2.55± 4.42

3.2 Sources of SO_2

We looked into the time series of SO_2, CO, Absolute Humidity and CO_2 and identified those events where we saw an enhancement in SO_2. The events can be broadly classified into two types: First, entrainment of SO_2 rich air during the breakdown of the nocturnal boundary layer and second, direct emission from combustion sources.

3.2.1 Entrainment of SO_2 rich air during the breakdown of nocturnal boundary layer

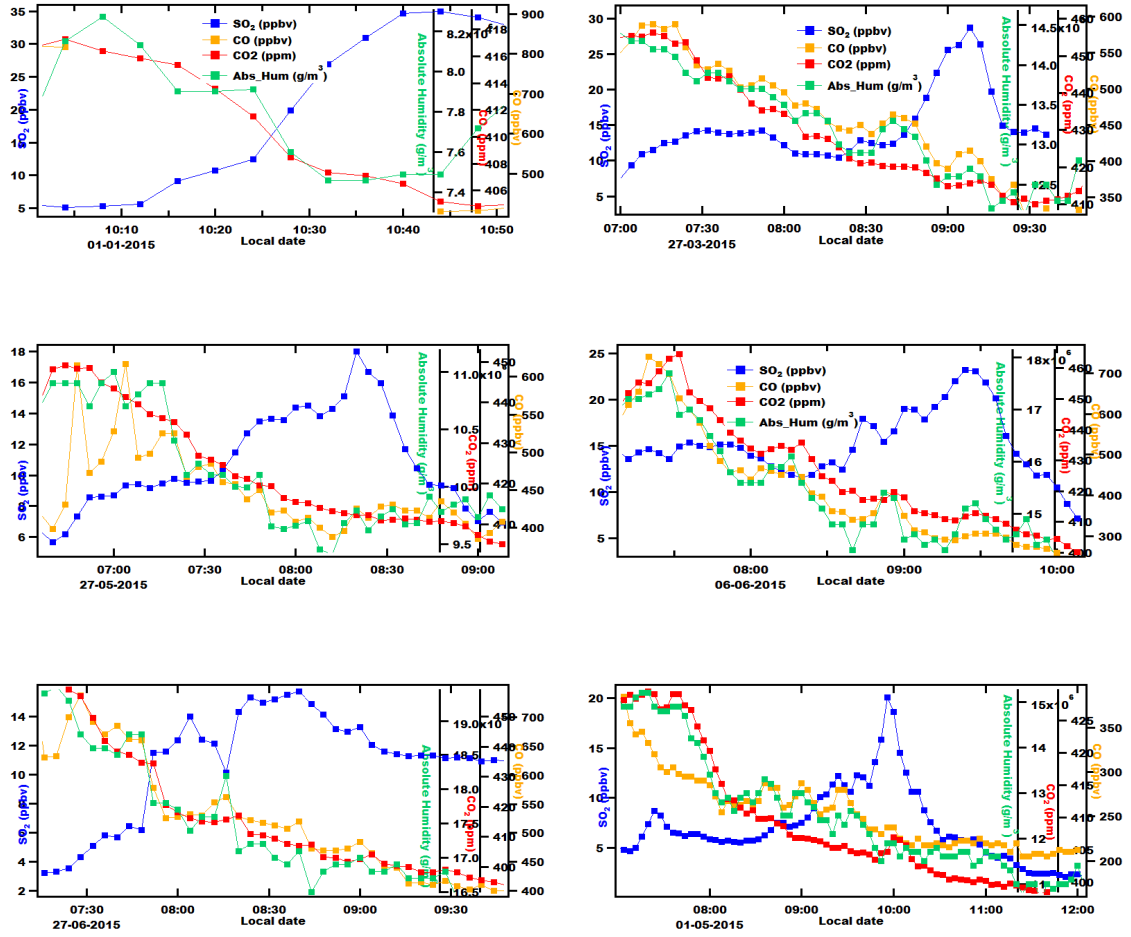

Figure 3.2: Time series of the six events in which enhancement in SO_2 was observed during the breakdown of nocturnal boundary layer

Figure 3.2 shows type 1 events for a period from January 2015 to December 2015. Six events were observed in which we see an enhancement in SO_2, accompanied by a decrease in absolute humidity, CO and CO_2. The emissions released at night from the power plants typically rise above the stable surface layer and tend to remain highly concentrated in the

vertically stratified residual layer. In the morning when the boundary layer breaks, the air in the residual layer mixes down, and thus we see an enhancement in SO_2. Since the air in the higher layer of the atmosphere is dry compared to that in the ground level, absolute humidity levels decrease when mixing occurs. The sources of CO and CO_2 are predominantly ground based, so when mixing happens CO and CO_2 undergo dilution, and their concentrations drop.

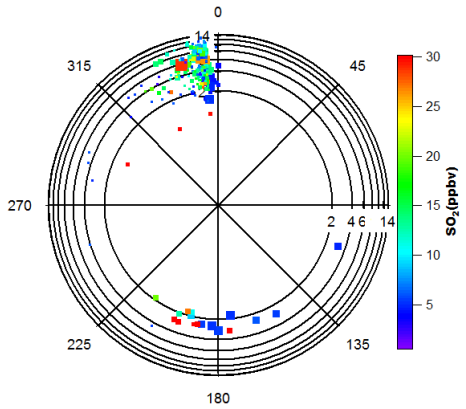

Figure 3.3: Polar plot of all the events during the breaking of nocturnal boundary layer. The radius represents the wind speed and the angle represents the wind direction. It is colour coded according to SO_2 and the marker size represents the NO.

Figure 3.3 shows the polar plot of all the six events mentioned above that helps the spatial identification of emission sources. The emissions come from North-West, South- East and South-West directions which is in agreement with the three coal powered power plants located at those directions. The power plants located at the South-East and South-West have a stack height of 200 m and it emits directly into the residual layer at night. The one which is in the North-West direction has a shallow stack height (60 m), but is located in a valley where the inversion would be more shallow. As a consequence it can still emit into the residual layer.

Figure 3.4 shows the summary of all the six events. It shows the variation in SO_2 and absolute humidity with the sunrise time which helps elucidate the enhancement in SO_2 due to the breaking of nocturnal boundary layer. It can be clearly seen that typically one to two hours after the sunrise, the concentration of SO_2 increased and the absolute humidity level dropped. The mean SO_2 levels increased from 5 ppb to 15 ppb and the mean absolute

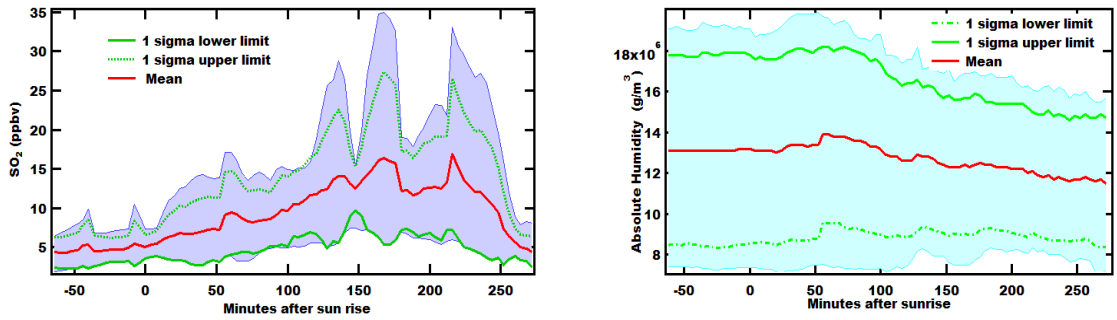

Figure 3.4: Variation in SO_2 and absolute humidity with the sunrise time. The top and bottom shaded region show the maximum and minimum respectively.

humidity levels dropped from 14 μg/m^3 to 12 μg/m^3.

3.2.2 Combustion sources of SO_2

In the second type of events, i.e, combustion events, the enhancements in SO_2 was accompanied by an increase in CO_2. These events are due to the direct emission from the combustion sources, and we calculated the combustion efficiency of those events. Combustion efficiency is defined as the molar ratio of carbon dioxide emitted to the total moles of carbon emitted.

Modified Combustion efficiency, MCE = $\triangle CO_2/(\triangle CO_2+\triangle CO)$[24]

For these events, we made a plot of SO_2 vs. NO as shown in figure 3.5 (left) and colour

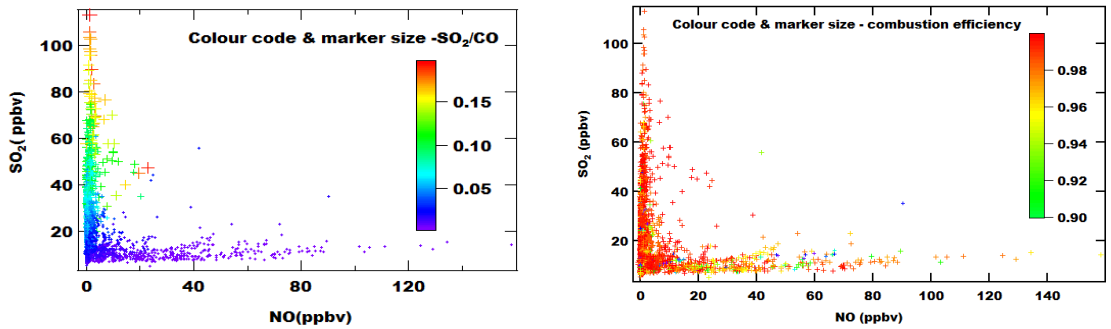

Figure 3.5: Plot of SO_2 vs NO for efficient combustion. (Left) The colour code and marker size represents the SO_2/CO ratio. (Right) The colour code and marker size represents the combustion efficiency.

coded it according to SO_2/CO emission ratio. SO_2 and CO have some emission sources in common and the ratio reflects the difference in source compositions. It is very clear from the plot that there are two types of combustion sources based on SO_2/CO emission ratio. First one is having a very low SO_2/CO ratio (<0.05), moderate SO_2 and typically high NO.

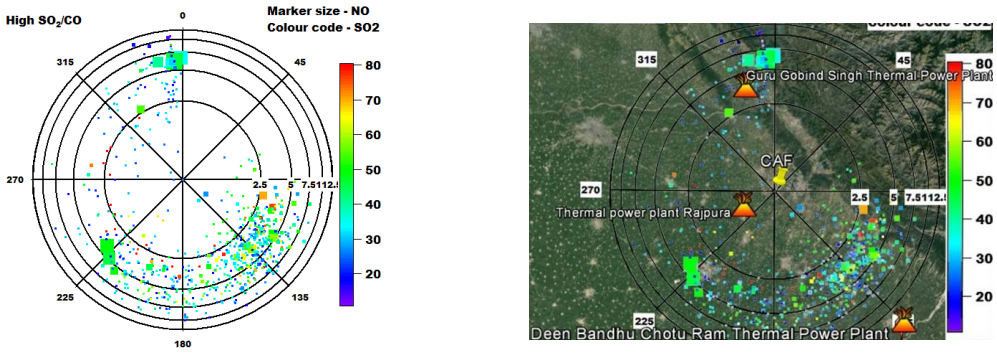

Figure 3.6: (Left) shows the polar plot of sources having $SO_2/CO > 0.05$ and (Right) shows the same polar plot overlaid on google earth. The radius of the plot represents the wind speed and the angle represents the wind direction.

The second source is having a very high SO_2/CO ratio ($\geqslant 0.05$), extremely high SO_2, and low NO.

Figure 3.5 (right) shows the SO_2 vs. NO plot colour coded with the combustion efficiency. While the colour coding with SO_2/CO ratio seems to suggest two dominant sources, combustion efficiency is more variable indicating that efficiency of combustion changes with operating conditions while the sulphur content of fuels do not change and as a consequence SO_2/CO emission ratio are less variable than the combustion efficiency.

Figure 3.6 shows the variation in SO_2 concentrations of high SO_2/CO combustion source as a function of wind direction and wind speed. From the plot, we can see that high SO_2/CO source has clearly three directions, South-East, South-West and North-West. The image overlaid on google earth clearly shows that the main source of these events are coal and most of it is coming from the three power plants which are located at the directions mentioned above. The three power plants are Rajpura thermal power plant which is located in the South-West direction, Guru Gobindh Singh thermal power plant which is located at the North-West wind sector and Chotu Ram thermal power plant which is located at the South east wind sector.

Figure 3.7 shows the diel box and whisker plot of type 1 combustion events. The SO_2 levels were higher during the late night and early morning. During the middle of the day SO_2 values were low due to dilution.

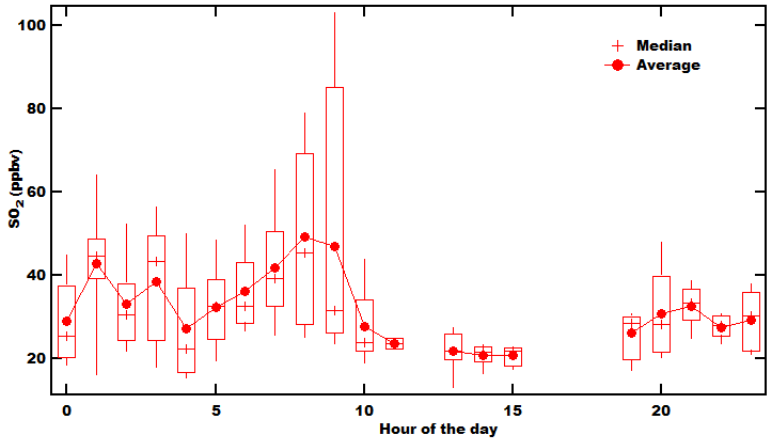

Figure 3.7: Diel box and whisker plot of high SO_2/CO source.

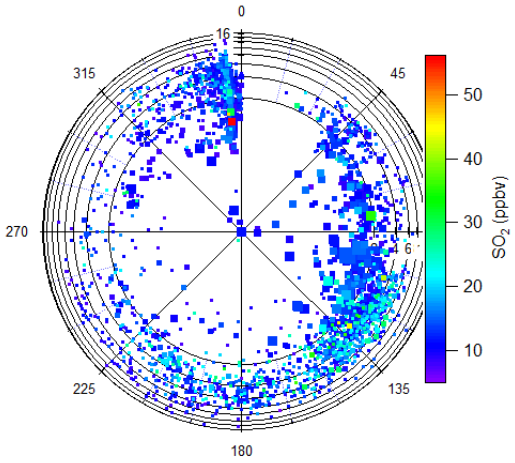

Figure 3.8: Polar plot of sources having SO_2/CO < 0.05. It is colour coded according to SO_2 and the marker size represents NO.

Figure 3.8 shows the polar plot of type 2 combustion source having SO_2/CO < 0.05. The source of this type of events are present in all the wind sectors. Figure 3.9 shows the diel box and whisker plot of this type of events. SO_2 levels were higher during the morning (5 am to 10 am) and evening (7 pm to 2 am).

We looked into the time series of these events and identified those events where we see an enhancement in SO_2, CO and CO_2. Twenty four events were identified in this type. Out of these 24 events, three types were observed.

In type 1, SO_2 showed good correlation with higher aromatics and benzene. For those events, we calculated the emission ratio of aromatics to benzene. Figure 3.10 shows the polar graph of type 1 events which has a toluene to benzene ratio of 2.6. The fetch region

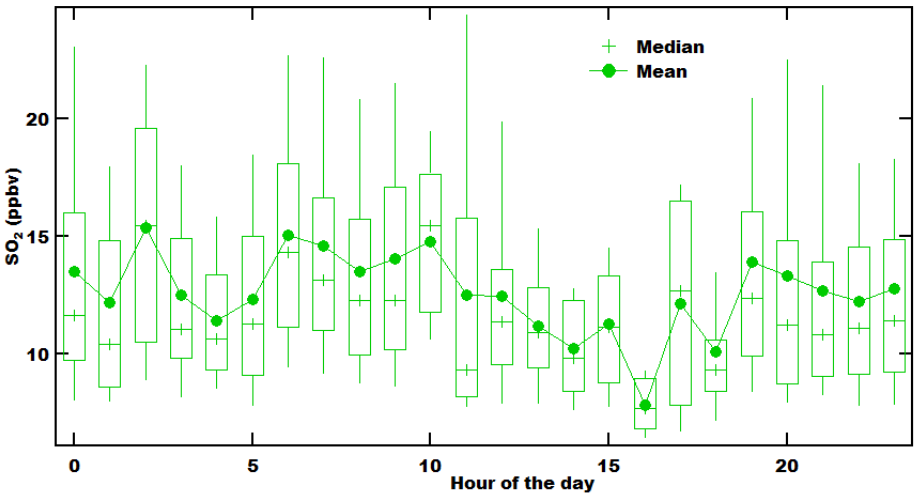

Figure 3.9: Diel box and whisker plot of low SO_2/CO source.

Table 3.2: Emission ratios to benzene for type 1 events

ERs/Benzene	In my study	Tunnel study, Hong Kong[25]
Toluene	2.6	2.27
C8-aromatics	0.86	0.87
C9-aromatics	0.40	0.77

for these events lie between $350°C$ to $135°C$ which is the wind sector where the road in front of the measurement site is situated. Table 3.2 shows the emission ratios to benzene of type 1 events. The emission ratios which we got are in good agreement with ratios from vehicular emissions reported by previous studies. Therefore the source of type 1 event is traffic. Figure 3.11 shows the polar plot of type 2 events. The emissions are coming from the region where the Rajpura power plant is situated. It has a toluene to benzene ratio of 0.85.

$$\ln((C_T^{'})/(C_B^{'})) - ln(C_T/C_B) = (k_B - k_T)[OH](t_2 - t_1) \qquad .....(3.2)$$

where $C_T^{'}/C_B^{'}$ and (CT/CB) are the measured ratios of toluene to benzene at the measurement site and at the source respectively, k_B and k_T are the temperature-corrected rate constants of the reaction of benzene and toluene with hydroxyl radical respectively and $(t_2 - t_1)$ is the transport time required by the air parcel to traverse from the source to the receptor site.

If we photochemically age a plume emitted from the power plant by 12 hours using equation 3.2, we get a toluene to benzene ratio of 0.7 which is comparable with the type 2 event

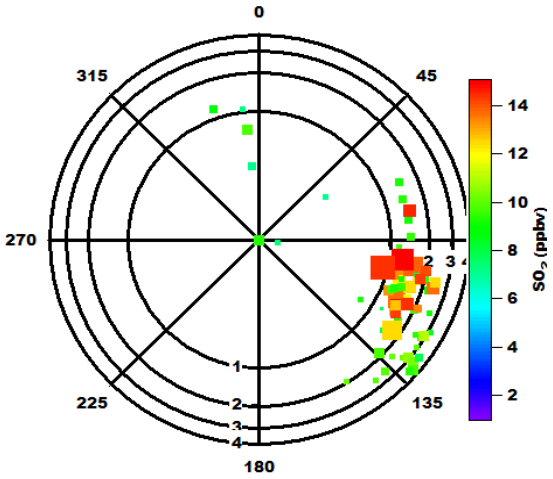

Figure 3.10: Polar plot of type 1 source

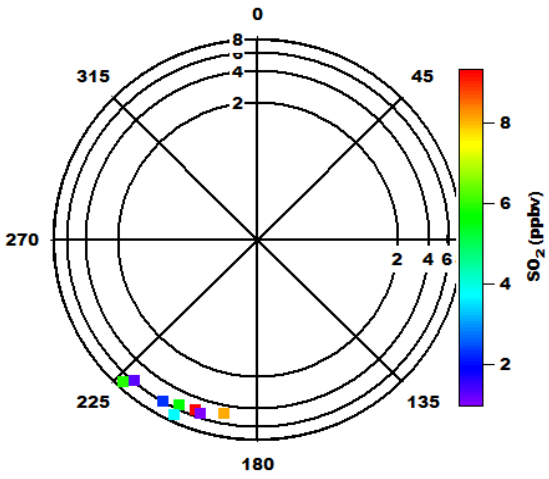

Figure 3.11: Polar plot of type 2 source

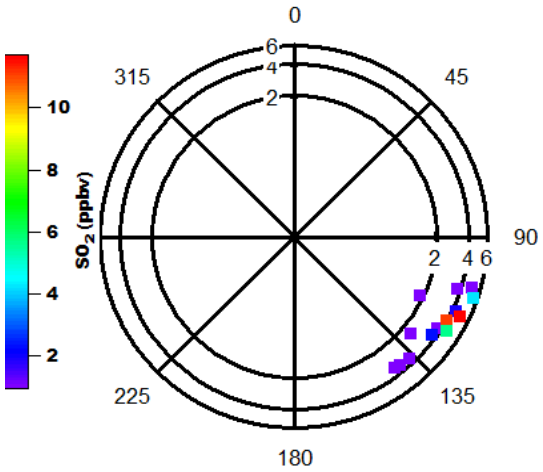

Figure 3.12: Polar plot of type 3 source

ratio. As the NO levels of type 2 events were very low (less than 1 ppbv) it is possible that this is an aged plume. So the type 2 events could be aged plumes coming from the Rajpura power plant.

The type 3 events has a toluene to benzene ratio of 1.0. Figure 3.12 shows the polar plot of these events. The emissions are coming from the South-East direction. As the NO levels were less than 1 ppbv, this could be aged plumes. The sources of this type of event is not clear.

3.3 Conclusion

The major sources of SO_2 measured at our site are the three power plants located at the North-West, South-West and South-East directions and traffic is also another source. Out

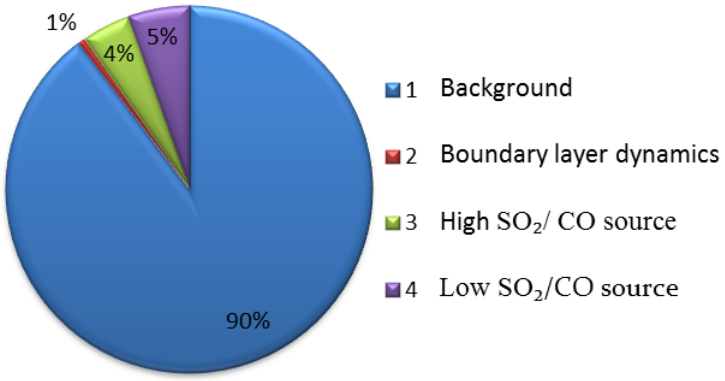

Figure 3.13: Contribution of SO_2 from different sources

of the total mass of SO_2 (1804 g) detected in the year 2015, 90% is not associated with fresh emissions or plumes, 5% is from sources with a low SO_2/CO ratio, 4% is from high SO_2/CO source and 1% is entrained from the troposphere due to boundary layer dynamics. Out of the total SO_2, only 5% can be attributed directly to the three power plants situated near the site with an installed capacity of 1400 MW, 1260 MW and 600 MW.

Lu et al., cast doubt on surface measurements in India. We find that power plant SO_2 due to the elevated release height, rarely impacts nearby surface sites. As a consequence decreasing surface mixing ratios and increasing SO_2 mixing ratios in the nocturnal residual layer and free troposphere are not mutually exclusive.

Bibliography

[1] T. Ohara, H. Akimoto, J. Kurokawa, N. Horii, K. Yamaji, X. Yan, and T. Hayasaka. An asian emission inventory of anthropogenic emission sources for the period 1980–2020. *Atmospheric Chemistry and Physics*, 7(16):4419–4444, 2007.

[2] Robert J Downing, Ramesh Ramankutty, and Jitendra J Shah. *Rains-Asia: an assessment model for acid deposition in Asia*. World Bank Publications, 1997.

[3] Daniel J. Jacob. *Introduction to atmospheric Chemistry*. Princeton University Press, January 1999.

[4] G. Myhre, D. Shindell, F.-M. Breon, W. Collins, J. Fuglestvedt, J. Huang, D. Koch, J.-F. Lamarque, D. Lee, B. Mendoza, T. Nakajima, A. Robock, G. Stephens, T. Takemura, and H. Zhang. *Anthropogenic and Natural Radiative Forcing*, book section 8, page 659 to 740. Cambridge University Press, Cambridge, United Kingdom and New York, NY, USA, 2013.

[5] Robert J Charlson, SE Schwartz, et al. Climate forcing by anthropogenic aerosols. *Science*, 255(5043):423, 1992.

[6] L Land, J Rosenfeld Mosher, and T Rowe. Mount pinatubo aerosols, chlorofluorocarbons, and ozone depletion. *Science*, 257:28, 1992.

[7] S Self, R Gertisser, Th Thordarson, MR Rampino, and JA Wolff. Magma volume, volatile emissions, and stratospheric aerosols from the 1815 eruption of tambora. *Geophysical Research Letters*, 31(20), 2004.

[8] Zifeng Lu, David G Streets, Benjamin de Foy, and Nickolay A Krotkov. Ozone monitoring instrument observations of interannual increases in so2 emissions from in-

dian coal-fired power plants during 2005–2012. *Environmental science & technology*, 47(24):13993–14000, 2013.

[9] Jonathan Williams Peter Warneck. *The Atmospheric Chemists Companion*. Springer, 2012. page no:71.

[10] PS Liss, G Malin, and SM Turner. Production of dms by marine phytoplankton. *Dimethyl sulphide: oceans, atmosphere and climate. Kluwer Academic, Dordrecht*, pages 1–14, 1993.

[11] ED Sofen, B Alexander, and SA Kunasek. The impact of anthropogenic emissions on atmospheric sulfate production pathways, oxidants, and ice core δ 17 o (so 4 2–). *Atmospheric Chemistry and Physics*, 11(7):3565–3578, 2011.

[12] Barbara J. Finlayson-Pitts. *Chemistry of the upper an dlower atmosphere theory,experiments and applications*. San Diego,Academic Press, 2000.

[13] D.R. Middleton L. Luhana and R.S. Sokhi. Oxidation of so2 and nox in plumes. Technical report, Environment Agency, Rio House, Waterside Drive, Aztec West, Almondsbury, Bristol, BS32 4UD, •.

[14] Chun-Hung Chang Wen Chao, Jun-Ting Hsieh and Jim Jr-Min Lin. Direct kinetic measurement of the reaction of the simplest criegee intermediate with water vapor. *Science*, 2015.

[15] S. Smolander M. Boy, D. Mogensen. Oxidation of so2 by stabilized criegee intermediate (sci) radicals as a crucial source for atmospheric sulphuric acid concentrations. *Atmos. Chem. Phys. Discuss*, 2012.

[16] JR Pierce, MJ Evans, CE Scott, SD D'Andrea, DK Farmer, Erik Swietlicki, and DV Spracklen. Weak global sensitivity of cloud condensation nuclei and the aerosol indirect effect to criegee+ so 2 chemistry. *Atmospheric Chemistry and Physics*, 13(6):3163–3176, 2013.

[17] Steven J Smith, J van Aardenne, Zbigniew Klimont, Robert Joseph Andres, A Volke, and Sabrina Delgado Arias. Anthropogenic sulfur dioxide emissions: 1850–2005. *Atmospheric Chemistry and Physics*, 11(3):1101–1116, 2011.

[18] J Kurokawa, T Ohara, T Morikawa, S Hanayama, G Janssens-Maenhout, T Fukui, K Kawashima, and H Akimoto. Emissions of air pollutants and greenhouse gases over asian regions during 2000–2008: Regional emission inventory in asia (reas) version 2. *Atmospheric Chemistry and Physics*, 13(21):11019–11058, 2013.

[19] Z Klimont, Steven J Smith, and Janusz Cofala. The last decade of global anthropogenic sulfur dioxide: 2000–2011 emissions. *Environmental Research Letters*, 8(1):014003, 2013.

[20] V. Sinha, V. Kumar, and C. Sarkar. Chemical composition of pre-monsoon air in the indo-gangetic plain measured using a new air quality facility and ptr-ms: high surface ozone and strong influence of biomass burning. *Atmospheric Chemistry and Physics*, 14(12):5921–5941, 2014.

[21] Hideo Okabe, Paul L Splitstone, and Joseph J Ball. Ambient and source so2 detector based on a fluorescence method. *Journal of the Air Pollution Control Association*, 23(6):514–516, 1973.

[22] Winston T Luke. Evaluation of a commercial pulsed fluorescence detector for the measurement of low-level so2 concentrations during the gas-phase sulfur intercomparison experiment. *Journal of Geophysical Research: Atmospheres*, 102(D13):16255–16265, 1997.

[23] Cavity ring-down spectroscopy (crds) — picarro.

[24] CE Stockwell, PR Veres, J Williams, and RJ Yokelson. Characterization of biomass burning emissions from cooking fires, peat, crop residue, and other fuels with high-resolution proton-transfer-reaction time-of-flight mass spectrometry. *Atmospheric Chemistry and Physics*, 15(2):845–865, 2015.

[25] KF Ho, SC Lee, WK Ho, DR Blake, Y Cheng, YS Li, Steven Sai Hang Ho, K Fung, PKK Louie, and D Park. Vehicular emission of volatile organic compounds (vocs) from a tunnel study in hong kong. *Atmospheric chemistry and physics*, 9(19):7491–7504, 2009.